Supplementary material: S1 Insight gained from experiments

1. Analog experiments

Sand box experiments proved to be particularly useful for the study of thin-skinned tectonic styles although there are limitations regarding replicability of results and the direct up-scaling of model results to geological structures [312]. Despite similarities in model results from a benchmark test involving 15 laboratories, [312] found that the frictional behavior of sand is highly sensitive to the preparation of the experiment. Thus also surface slopes and spacing of thrusts obtained in experiments must not be overinterpreted. Nevertheless, analog experiments by [291] that analyzed frictional versus viscous décollements revealed that strong frictional décollements (representing for example shales) produce forward verging thrust faults that develop in-sequence toward the foreland (see Figure 1). Weak viscous décollements (representing evaporites) on the other hand result in more symmetrical box folds (Figure 1) that form simultaneously across the entire fold belt. In these experiments, thrust faults developed in the brittle cover above the frictional décollement only; they are associated with forward verging folds (hanging-wall ramp anticlines at the front, footwall ramp synclines at the rear). Those thrust faults with a high displacement produced backward verging folds in the central part of the thrust sheets.

Figure 1 Analog models showing contrast between strong frictional (shale type) and viscous (evaporitic) décollements. Shortening occurs in response to a moving rigid vertical wall at the right side of the sandbox. Redrawn from [291].

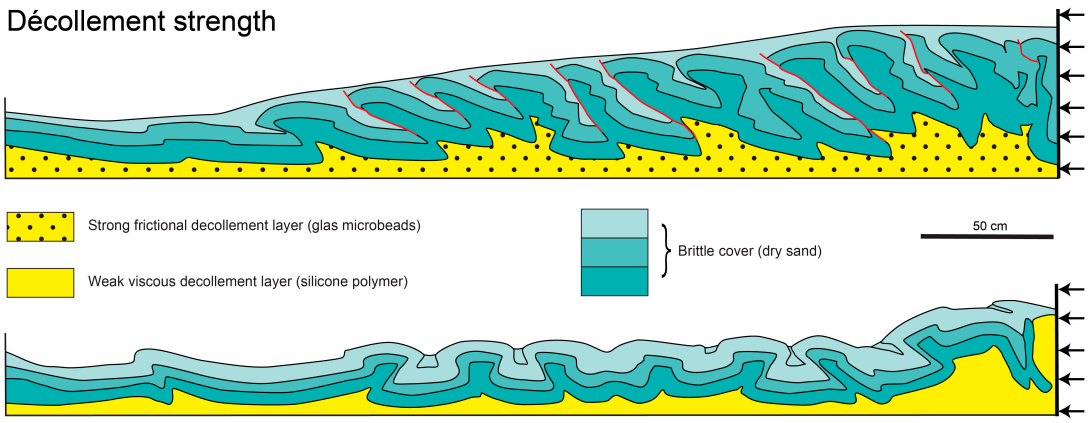

A topic addressed by a number of papers concerns the inversion of basins and the potential reactivation of syn-sedimentary normal faults in compression. [313] and [49] modeled the behavior of graben or rift structures in compression.

[49] modelled the formation of a symmetric rift followed by coaxial compression and associated inversion of the rift. The rheological layering of the crust was modeled as a brittle upper crust, a semi-brittle middle crust and a weak lower crust. In the model, the upper crust was represented by pre-rift and syn-rift sediments consisting of dry aeolian quartz sand (with ⌀ = 30°). For the middle crust, high-viscosity silicone putty was used (with a viscosity of 4×105 Pa s at 23 °C and modeling strain rate), while the lower crust was modeled with low-viscosity silicone

putty (with a viscosity of 3×104 Pa s at 23 °C and modeling strain rate). Layering is rendered visible for X-ray computer tomography by magnetic markers. The experiment was designed to develop a transfer zone parallel to the extension and shortening direction in the center of the sand box.

The cross-section shown in Figure 2 is from experiment 1 (M17, cross-section a) of [49] and is located outside the influence of the transfer zone. The cross-section shows the final state after 2.5 cm of extension followed by 5 cm of shortening. Three types of faults may be discerned in the antiformal dome: reactivated normal faults associated with the incipient rift, newly formed reverse faults outside the incipient rift, and newly formed normal faults at the top of the dome within the syn-rift sediments. Upwelling of the modeled weak crust in the core of the dome occurred already in the early stages of shortening and continued throughout the inversion. An important result of this upwelling is the rotation of the normal faults within the rift and namely the rift-margin fault from a steep dip of 60 to 65° to less than 45° near the end of the experiment. The displacement along these faults is relatively modest, apart the two closely spaced within-rift faults above the rift-margin fault on the left side. New reverse faults formed outside the rift, the first ones right next to the rift-margin faults, the following successively farther away. The normal faults at the top of the dome formed in the latest stage of inversion as a result of extension related to updoming, All in all it seems that much of the inversion involved a passive rotation of the modeled upper and middle crust owing to upwelling of the lower crust. The small scale folds visible between the reactivated faults and the new reverse fault indicate that the material between the faults was extended in a direction parallel to the faults, which contributes to the upward escape of material in the course of inversion.

Figure 2 Inversion of a symmetric rift. Redrawn from [49; their experiment 1 [M17]].

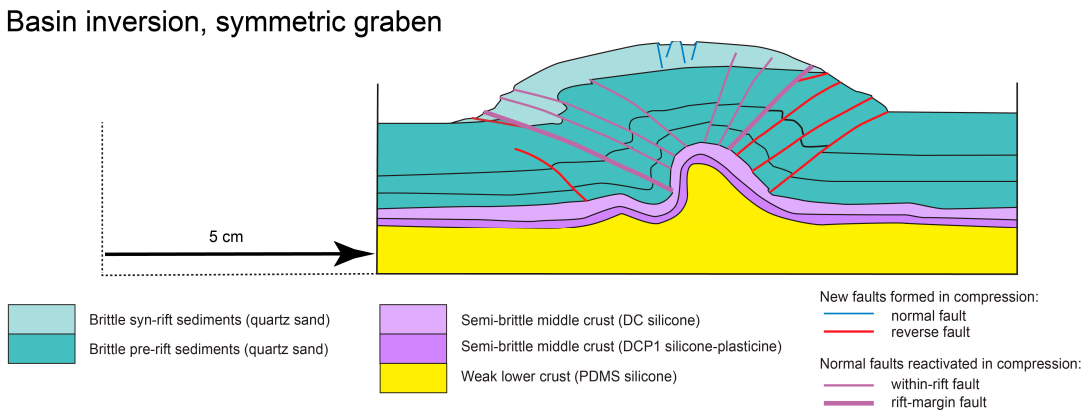

[313] investigated the effect of the mechanical properties of the graben fill and the incipient geometry of an asymmetric graben upon the style of deformation during coaxial shortening and inversion. Pre- and post-rift sediments were modeled using layers of quartz and corundum sand, which have similar mechanical properties but different attenuation for X-rays and thus render the analysis by non-destructive X-ray computer tomography possible. The quartz sand used has an initial internal friction angle of ϕ = 35.5° that reduces to 31.2° by strain softening; for corundum sand ◎◎reduces from 37° to 32.2°, for microbeads from 22.3° to 20.6°.

[313] found that the reactivation of syn-rift normal faults was minor and limited to the graben bounding faults (see Figure 3). The one closer to the mobile wall was slightly reactivated and propagated through the post-rift sediments at a shallow angle. In the course of inversion, new back-thrusts developed in-sequence outside the graben. On the opposite side of the graben, the graben-bounding fault was not reactivated, but a shear zone developed parallel to this fault within the weak graben fill. This shear zone widened successively into the center of the graben

fill in later stages of inversion, its upper limit moving from position 1 to 3 in Figure 3. This resulted in a fold with an inverted limb and is responsible for the extrusion of the graben fill as highlighted by the motion of the reference points (c moves passed a and b).

Figure 3 Inversion of an asymmetric graben with a weak graben fill. Redrawn from [313; their NG model)]

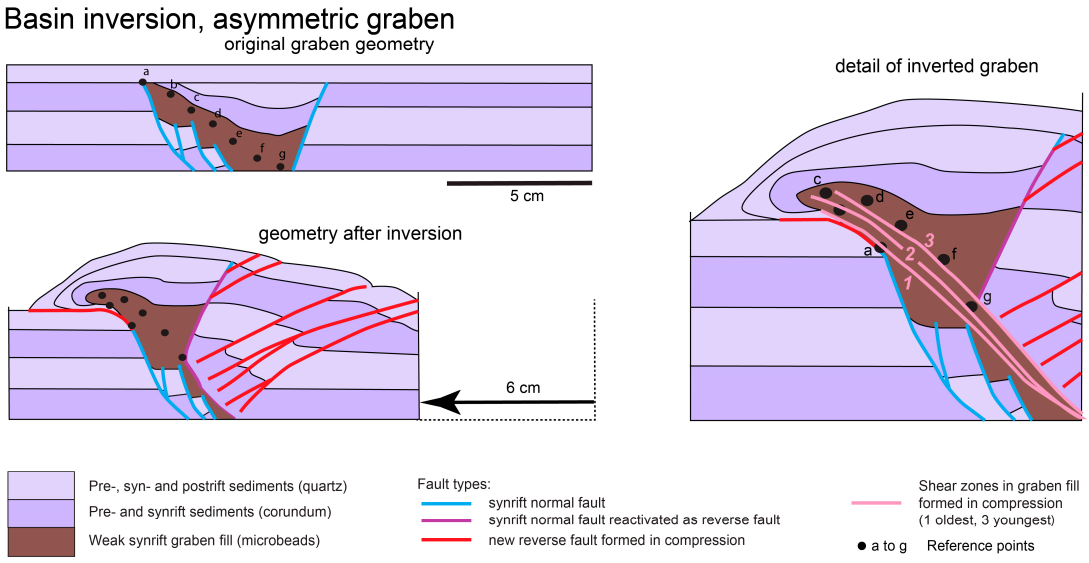

2. Numerical experiments

There is a rich literature of numerical experiments on thin-skinned tectonic styles in fold-and-thrust belts (see e.g. review by [214]). Critical taper theory has received a particular attention, even though the analytical solution of this theory considers a homogeneous material on the verge of brittle failure throughout the wedge [54,55]. Numerical experiments go beyond these conditions and include heterogeneities within the wedge and surface processes (erosion or sedimentation). Studies on thin-skinned style tectonics consider taper angle, dip angle of the basal décollement, strength of the material forming the basal décollement, strength of the wedge-internal material, length of thrust sheets, dip of pro- and back-thrusts and surface erosion to name the most important parameters. Several codes exist to perform the actual calculations. These are compared to each other and to analog experiments in benchmark tests by [315].

[316] studied the influence of the frictional strength of a décollement horizon on the shape of the evolving taper. The décollement horizon was either frictional with the basal frictional strength ⊚b varying between 5 and 25° (representing shale) or viscous (representing salt) with viscosities ⊚b ranging from 1e17 to 1e19 Pa·s. The detached cover, as well as the syntectonic sediments added by diffusion were treated with a viscoelastoplastic behavior with a frictional angle ϕ of □30°. Frictional basal décollement led to the formation of asymmetric forward verging folds associated with thrust faults. Higher values of ⊚⊚⊚yields tapers with steeper surface slopes and lower dip angles of thrust faults. The deformation front in these experiments propagates towards the front. Figure 4 shows the final stage of the experiment with a frictional décollement of $\phi_{⊚}$ = 10°. Individual thrust faults propagate off the basal detachment upward into the inverted limbs between anticlinal and synclinal hinges and broaden to shear zones in towards the top. This behavior is reminiscent of what is called fault-propagation folding by [317].

Viscous décollements (not shown here) result in symmetrical folds verging forward and backward, similar to the analog experiments reported by [291] shown in Figure 1.

Figure 4 Numerical model using a frictional décollement (shale) with ϕ_b= 10°. Redrawn from [316] The dotted line inclined at 3.4° corresponds to the analytical solution derived for critical taper theory.

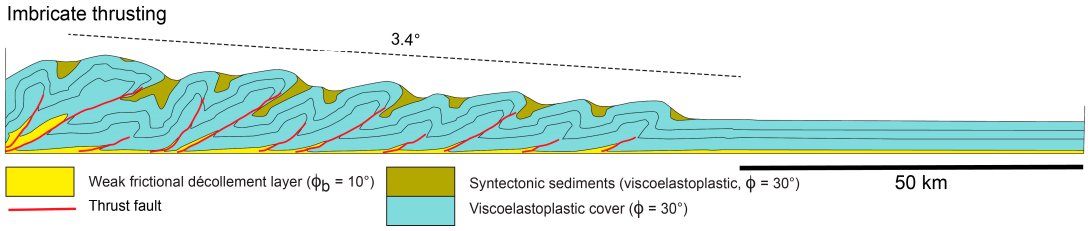

[311] modelled thin-skinned fold-and-thrust belts including flexural isostatic subsidence, one or two weak décollement layers, strong layers undergoing strain softening and syntectonic sedimentation or erosion. Their model 4 is shown in Figure 5 in a simplified fashion. Model 4 involves two very weak décollement layers and the strong layers above these décollements become weaker with ϕ_{eff} decreasing from 38 to 18°. Diffusive sedimentation fills steeply bounded depressions forming at the model surface. In the early stages of the experiment the wedge thickens by pop-up structures bounded by oppositely dipping shear zones. Later, these pop-ups get deformed and the wedge grows by frontal accretion whereby the upper strong layer thickens by imbricate thrusting independently from the lower strong layer. The individual imbricate thrusts emanate from the décollement layer, ramp up through the upper strong layer and form fault-propagation folds at their tip. Still later, the lower strong layer is shortened by thrust faults that emanate from the lower décollement layer and virtually double stack the strong layer. These thrust sheets are longer than the ones in the upper layer. The latter are carried passively by the underlying thrust sheets as they slide along the lower décollement layer. At the front of the thrust sheet, the lower strong layer is thrust onto the upper strong layer causing a topographic relief.

Figure 5 shows the final state of model 4 after 210 km of shortening. Imbricate thrusting and fault-propagation folds above the undeformed lower strong layer are discernible at the front of the wedge in the upper strong layer. Long thrust sheets occur farther back in the lower strong layer. Their formation postdates the imbricate thrusting in the overlying upper strong layer. [311] present a model with three décollement layers (their model 7) where the same sequence of thrusting is observed. In that model the lowermost strong layer undergoes thrusting in a more internal part and later than the middle strong layer. It thus seems that the modeled wedges attain their taper shape by sequential thrusting which involves the top of wedge first and only later affects the bottom of the wedge. A similar observation was made by [316] in the case where the lower detachment is weaker (ϕ_b = 5°) that the upper detachment (ϕ_m = 10°).

Figure 5 Numerical model with two very weak detachments separating two strong layers which undergo strain softening. Simplified from [311; their model 4].

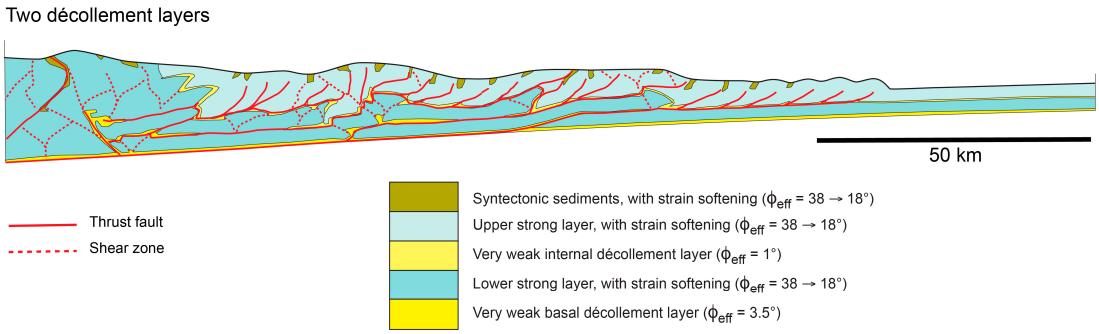

[316] modelled a continent-continent collision involving the entire lithosphere. They used thermo-mechanically coupled frictional-plastic and thermally activated power-law viscous rheologies. Their pure contractional model (M2) shown in Figure 6 yields both, a thick- and a thin-skinned style combined. In the course of the experiment, the deformation front migrates towards the external part. Thin-skinned deformation is driven by thick-skinned deformation. Each of the thrusts emerging from the upper crust pushes the pre-rift sediments towards the foreland. The décollement layer at the base of the pre-rift sediments is thereby activated and thrusts develop within the pre-rift sediments. At the rear of the emerging thrusts the décollement layer is deactivated. Thrust faults within the pre-rift sediments have little or no influence on crustal faults. The crustal faults level off near the limit to the lower crust owing to the up-scaled viscosity in the latter.

Figure 6 Numerical model of a continent-continent collision with a weak décollement layer at the base of pre-rift sediments and a viscosity contrast between upper and lower crust. Simplified from [316; their model M2].

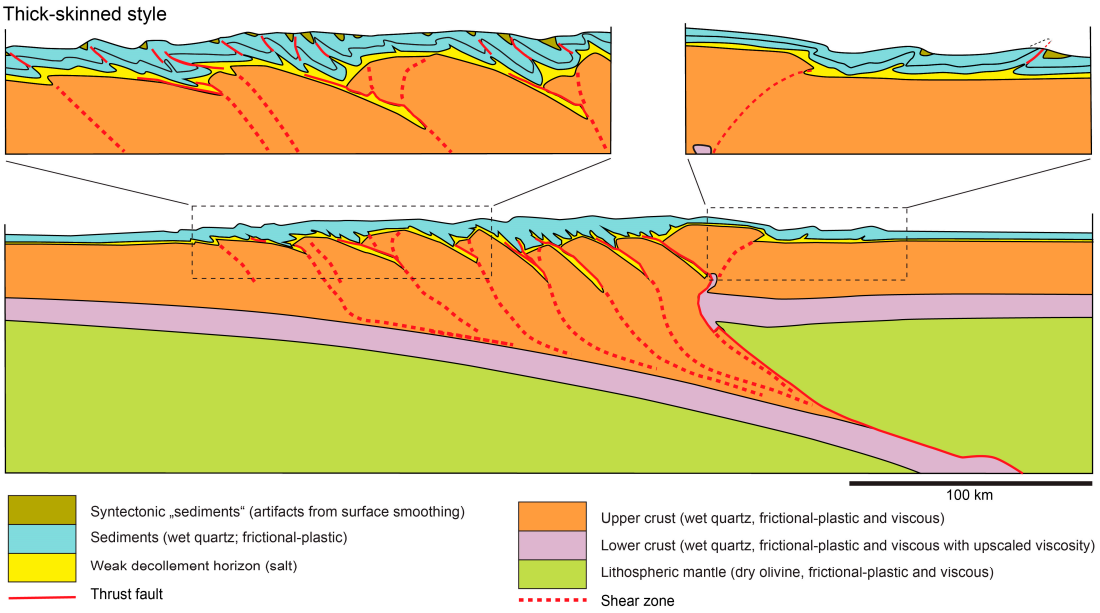

3. Summary

From natural examples and modeling results several factors may be identified that strongly control the deformational style of orogenic wedges.

(1) Décollement horizons with a thickness in excess of roughly half of the thickness of the overlying strong layer result in detachment folds. If the décollement layer is thinner the strong layer is detached by imbricate thrusting whereby the individual thrust faults end upward blindly in the core of folds.

(2) For relatively strong décollement layers with a frictional behavior (e.g. shale), the wedge grows by outward propagation of folding and/or thrusting and the associated folds have a proward vergence. A viscous behavior of the décollement layer (e.g. salt) on the other hand leads to a wider wedge where deformation occurs throughout the wedge and folds are more symmetrical [291,316].

(4) In case of multiple décollement layers, the uppermost is first activated; the next following start out in a more internal position, propagate outward and passively transport the fold-and-thrust structures of the earlier formed top most structures [311].

(5) Surface processes influence the internal structure of orogens significantly. In models involving the entire crust, syn-orogenic sedimentation enhances the formation of a thin-skinned type wedge by frontal accretion [44,310]. Erosion, on the other hand, leads to rock uplift and exhumation whereby also the deep structure of the orogen is affected [61,318]. The models by [60] suggest that changing wind directions (and precipitation rates) influence the asymmetry of the model orogen; [319] and [310] argue that erosion leads to strain localization owing to upward advection of hot material and to a narrower orogen. [44] found that erosion favors thick-skinned type basal accretion.

(5) Lateral discontinuities caused by rifting and weak basin fill exert an important influence upon compression. Although deformation concentrates near the rift bounding faults, the reactivation of steep normal faults is minor [313] or restricted to the early phase of inversion [49]. Many new reverse faults develop in the crust outside the basin. The actual expulsion of the weak basin fill starts with a vertical uplift of the entire basin. Activation of shear zones within the basin and parallel to the graben bounding fault raise the graben fill further and result in recumbent folds; at this stage the syn-rift faults are inactive.